

# ChemComm

Chemical Communications

Accepted Manuscript

This article can be cited before page numbers have been issued, to do this please use: Y. Li, X. Liu, W. Pan, N. Li and B. Tang, *Chem. Commun.*, 2020, DOI: 10.1039/C9CC08447A.



This is an Accepted Manuscript, which has been through the Royal Society of Chemistry peer review process and has been accepted for publication.

Accepted Manuscripts are published online shortly after acceptance, before technical editing, formatting and proof reading. Using this free service, authors can make their results available to the community, in citable form, before we publish the edited article. We will replace this Accepted Manuscript with the edited and formatted Advance Article as soon as it is available.

You can find more information about Accepted Manuscripts in the [Information for Authors](#).

Please note that technical editing may introduce minor changes to the text and/or graphics, which may alter content. The journal's standard [Terms & Conditions](#) and the [Ethical guidelines](#) still apply. In no event shall the Royal Society of Chemistry be held responsible for any errors or omissions in this Accepted Manuscript or any consequences arising from the use of any information it contains.

## Photothermal therapy-induced immunogenic cell death based on natural melanin nanoparticles against breast cancer†

Received 00th January 20xx,  
Accepted 00th January 20xx

Yanhua Li‡, Xiaohan Liu‡, Wei Pan, Na Li\* and Bo Tang\*

DOI: 10.1039/x0xx00000x

www.rsc.org/

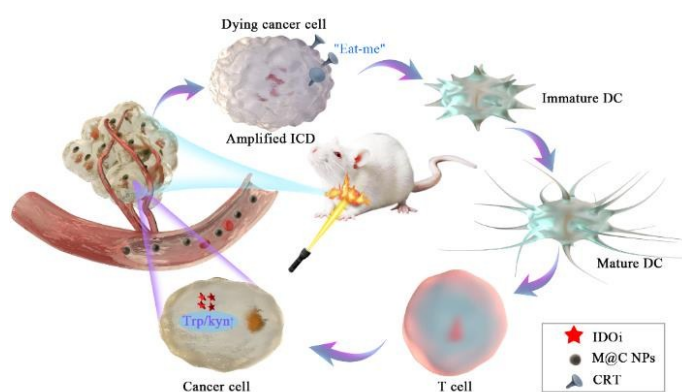
**A photothermal and immune co-therapy strategy based on the natural melanin nanoparticles was developed for treating the primary and abscopal breast cancer.**

Cancer immunotherapy, a remarkable cancer treatment, aims at stimulating or mobilizing the body's immune system to enhance the anti-tumor immunity, so as to control and damage cancer cells.<sup>1-3</sup> However, it is difficult to eliminate primary tumors relying on cancer immunotherapy alone due to low activation of immune response and typical immune escape of tumors.<sup>4-6</sup> One main reason for low activation of immune response is the weak immunogenicity during tumor occurrence and development.<sup>7</sup> So it is meaningful to enhance the immunogenicity of cancer cells and stimulate the immune response in tumor site specifically.

Immunogenic cell death (ICD), which releases damaged-associated molecular patterns (DAMPs), can provide “eat me” signals for the innate immune system to increase the immunogenicity.<sup>8,9</sup> Studies have shown that phototherapies, such as photodynamic therapy (PDT) or photothermal therapy (PTT), can cause the ICD of cancer cells.<sup>7,10</sup> Therefore, photodynamic or photothermal reagents with laser radiation can serve as therapeutic agents and immune response activators. Most used phototherapy reagents are inorganic semiconductor nanoparticles with poor biocompatibility, which are limited in clinical applications due to the immune clearance and side effects.<sup>11-14</sup> Compared to the synthetic composites, nanoparticles derived from endogenous materials are highly acclaimed in the applications of nanomedicine.<sup>15</sup> Melanin is a biological pigment, formed by a series of chemical reactions of tyrosine or 3, 4-dihydroxyphenylalanine, which widely exists in animals, plants and protozoans.<sup>16,17</sup> And melanin usually

presents in the form of aggregation with black color, such as melanin nanoparticle from cuttlefish, which has high photothermal conversion efficiency.<sup>18,19</sup> Such natural melanin nanoparticles with good biocompatibility are excellent candidates for PTT-induced ICD.

Herein, we designed a photothermal and immune co-therapy strategy based on natural melanin nanoparticles (M NPs) for treating breast cancer. Natural M NPs were obtained from cuttlefish as photothermal reagents, which were coated with cancer cell membrane (M@C NPs) to achieve homologous adhesion of tumor. The resulting M@C NPs exhibit much enhanced antitumor activity for three reasons. First, natural M NPs are black materials, which have UV-vis absorption at all wavelengths and possess excellent capability of photothermal conversion under irradiation of 808 nm. Second, camouflaged with membrane of 4T1 cells makes the M@C NPs as “smart bullet” to escape from immune clearance and homologously target to the tumor site. Third, additional immunoblocking inhibitor synergizes with PTT-induced ICD to inhibit the tumor immune escape and enhance antitumor immune response. This integrated strategy based on natural M NPs results in an increased amounts of CD8+ T cells and higher levels of cytokines, which eventually realizes the effective treatment of primary and abscopal tumors (Scheme 1).



**Scheme 1.** Schematic illustration of M@C NPs for cancer immunotherapy by ICD induction and immune checkpoint blockade.

College of Chemistry, Chemical Engineering and Materials Science, Key Laboratory of Molecular and Nano Probes, Ministry of Education, Collaborative Innovation Center of Functionalized Probes for Chemical Imaging in Universities of Shandong, Institute of Molecular and Nano Science, Shandong Normal University, Jinan 250014, P. R. China. E-mail: lina@sdu.edu.cn; tangb@sdu.edu.cn

† Electronic Supplementary Information (ESI) available: Experimental details and supplementary figures. See DOI: 10.1039/x0xx00000x

‡ These authors contributed equally to this work.

M NPs were collected from the ink sac of cuttlefish by differential centrifugation. Transmission electron microscope (TEM) image in Figure 1A shows that the M NPs have spherical morphology and good dispersibility (130-150 nm). After coated with 4T1 cell membrane, M@C NPs become adhesive and have a lipid layer on the surface (Figure 1B). The hydrodynamic size of M@C NPs ( $259 \pm 6$  nm, Figure 1D) is higher than that of M NPs ( $235 \pm 4$  nm, Figure 1C), demonstrating the successful coating of cell membrane. The results in Figure S1 show that M@C NPs have good dispersibility and long-term stability in PBS or mimicked interstitial fluid. To verify the membrane on the M NPs, western blotting assays were carried out. Four major proteins of cancer cell membrane associated with cell invasion and metastasis were studied.<sup>20</sup> It shows that these proteins remained their characteristics during the extraction and coating processes (Figure 1E). Fourier infrared absorption spectrum (FT-IR) shows that M nanoparticles have strong and broad FT-IR transmission peak at  $3300\text{ cm}^{-1}$ , which corresponds to O-H and N-H stretching. Consecutive aromatic bending (C=C, C=N) is at  $1600\text{ cm}^{-1}$  and carbonyl stretching (C=O) is at  $1350\text{ cm}^{-1}$ . The FT-IR transmission peak of M@C nanoparticles changed a little differently due to the complex components of cell membrane (Figure S2). Zeta potential values,  $-16.5 \pm 0.3$  mV for M NPs,  $-5.6 \pm 0.5$  mV for cell membrane and  $-10.8 \pm 0.2$  mV for M@C NPs, further evidenced the successful formation of nanoparticles (Figure 1F). M@C NPs have the same full band absorption as M NPs, which indicates the same optical property of M NPs and M@C NPs (Figure 1G). Excellent light absorption property provides good facilities for the subsequent PTT of M@C NPs.

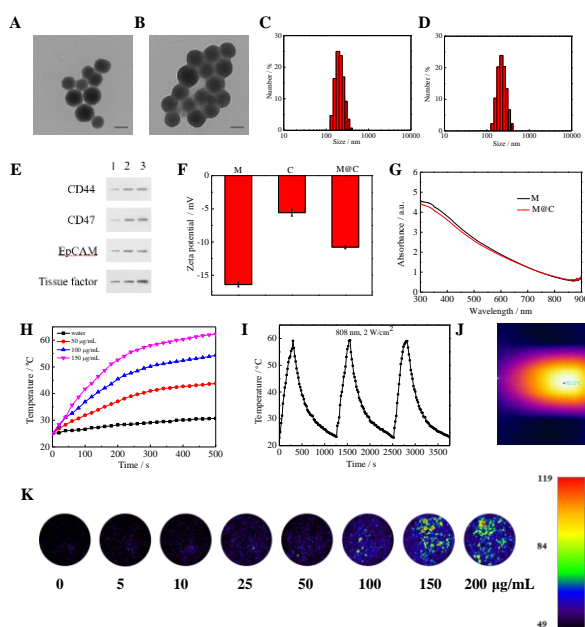


**Figure 1.** TEM images of M NPs (A), M@C NPs (B), scale bars are 100 nm. Hydrodynamic size distributions of M NPs (C) and M@C NPs (D). Western blotting assays of CD44, CD47, EpCAM and tissue factor: 1-3, 4T1 cells; cell membranes; M@C NPs (E). Zeta potentials of M NPs, cell membranes and M@C NPs (F). Absorption spectra of M NPs and M@C NPs (G). Temperature changes of M@C NPs under 808 nm laser ( $2\text{ W/cm}^2$ ) (H). Photothermal stability of  $150\text{ }\mu\text{g/mL}$  M@C NPs with three cycles (I). Photoacoustic images of  $150\text{ }\mu\text{g/mL}$  M@C NPs after laser irradiation (J). Photoacoustic images of M@C NPs (K).

The photothermal effect of M@C NPs was studied under continuous laser irradiation ( $808\text{ nm}$ ) at  $2\text{ W/cm}^2$  for 500 s. The temperature is related to both the exposure time and concentrations of M@C NPs (Figure 1H). The temperature rapidly rose to about  $60\text{ }^\circ\text{C}$  within 5 min and then remained stable with  $150\text{ }\mu\text{g/mL}$  M@C NPs, which is much higher than that of the water (Figure 1H, J). Moreover, the photothermal study of  $150\text{ }\mu\text{g/mL}$  M@C NPs with three cycles shows that M@C NPs have good photothermal stability (Figure 1I). The photothermal conversion efficiency of M@C NPs was calculated to be about 45%. All these results demonstrate the potential of M@C NPs for PTT. The photoacoustic signals of M@C NPs (0, 5, 10, 25, 50, 100, 150, 200  $\mu\text{g/mL}$ ) were measured. As Figure 1K shows, photoacoustic signals enhance with the increase concentration of the M@C NPs, which is in accordance with the photothermal property.

To verify the biocompatibility of M@C NPs, MTT assays were performed. When the concentration of M@C NPs reaches  $1000\text{ }\mu\text{g/mL}$ , the survival rate of cells is still above 90% (Figure S3), which shows the excellent biocompatibility. The cytotoxicity of M@C NPs under laser radiation was also studied. Laser (L) or M@C NPs (M@C) alone has little toxicity to cells, while M@C NPs under laser radiation led to massive cell death (cell viability less than 15%) (Figure S4). Above experimental results show that M@C NPs have good biocompatibility without laser radiation and have severe cytotoxicity with laser radiation, which are suitable for biological PTT.

Then the immunogenic cell death (ICD) of cancer cells through the PTT of M@C NPs was investigated. Calreticulin proteins (CRT) are the typical biomarker to characterize ICD.<sup>21,22</sup> When ICD occurs, CRT translocate from endoplasmic reticulum to the cytomembrane of dying cells and act as "eat me" signals to provoke an immune response.<sup>23</sup> Immunofluorescence assays (Figure 2A) showed that M@C NPs or laser alone didn't induce the high expression of CRT, which was in accordance with the results in Figure S4. M@C NPs or M NPs under laser radiation (M@C+L and M+L) induced the higher level of CRT than other groups, indicating their good photothermal effect. Moreover, the melanin nanoparticles coated with cell membrane have better cell fusion ability due to the homologous targeting of cancer cells, which results in more uniform fluorescence intensity of cells treated with M@C+L.

The cell invasion capacity of cancer cells was also studied. 4T1 cells were divided into five groups treated with M@C+L, M+L, M@C, L and PBS, respectively. The cell invasion capacity can be seen from the number of cells through transwell chambers. Few cells treated with M@C+L and M+L can pass through transwell chambers, which indicated that PTT can affect the physiological function of cancer cells (Figure 2B). The relative invasion numbers of cancer cells was also quantified and the data (Figure S5) is consistent with the above CRT results.

Subsequently, the targeting capability of M@C NPs was evaluated via photoacoustic imaging. M NPs or M@C NPs were intravenously injected into the tumor-bearing mice and the photoacoustic signal of tumors was measured at different time points. Photoacoustic signals at tumors treated with M@C NPs are much higher than that with M NPs, which indicates the

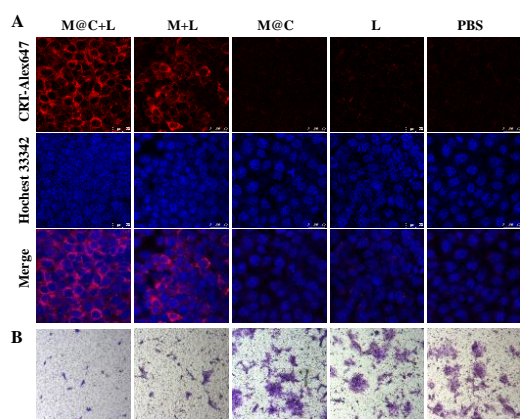


**Figure 2.** Expression of CRT proteins on the surface of 4T1 cells (A); Images of invasive cells with different treatments (B).

better tumor targeting ability of M@C NPs due to the homologous adhesion of cancer cell membrane (Figure 3A). The corresponding quantifications of photoacoustic signal of M NPs or M@C NPs are shown in Figure S6.

Photothermal images of mice were taken by an infrared imager after the irradiation (808nm) at 12 h post-injection. The temperature of tumors treated with M@C NPs was much higher than that treated with M NPs or PBS during the NIR irradiation for 5 min, which also shows that M@C NPs have better targeting ability to tumor than M NPs (Figure 3B). The above results show that M@C NPs are excellent candidates for PTT.

Indoleamine 2,3-dioxygenase (IDO) is highly overexpressed in tumor microenvironments to inhibit antitumor immune responses.<sup>24,25</sup> To block the immunity suppression, small-molecule IDO inhibitor INCB24360 (IDOi)<sup>26,27</sup> was applied to enhance the immune response. Interleukin-12 (IL-12) and interleukin-6 (IL-6) are secreted by relevant immune cells, which are applied to verify the immune response.<sup>28-30</sup> By enzyme-linked immunosorbent assay (ELISA), the secretion levels of IL-12 and IL-6 were low in group (iv) M@C+IDOi, (v) L and (vi) PBS, indicating that no immune response was activated (Figure S7A and B). And the level of IL-6 and IL-12 in group (iii) M+L+IDOi was higher than that in group (iv), (v) and (vi), which manifested that the immune response was provoked favourably. The tumor targeting ability of M NPs was much poorer than that of M@C NPs, so the effect of PTT was worse in group (iii) M+L+IDOi than that in group (ii) M@C+L. As expected, a remarkable increase of IL-12 and IL-6 in group (i) M@C+L+IDOi reflected the strong immune response, which indicated that the photothermal and immunological therapy can synergistically provoke the immune response. Moreover, immunofluorescent staining images showed that CD3+ and CD8+ T cells in tumors treated with M@C+L+IDOi are much more than other groups, which also suggested the stronger immune response in group (i) (Figure 3C). The quantification of the fluorescence signals is shown in Figure S8. The results were in accordance with that by ELISA. In addition, H&E stained images show that tumors of mice treated with M@C+L+IDOi represented the most severe tissue damage among six groups, which reflects the best therapeutic effect (Figure 3D). The above experimental results show that the ICD of cancer cells induced by PTT can serve as the immunogen,

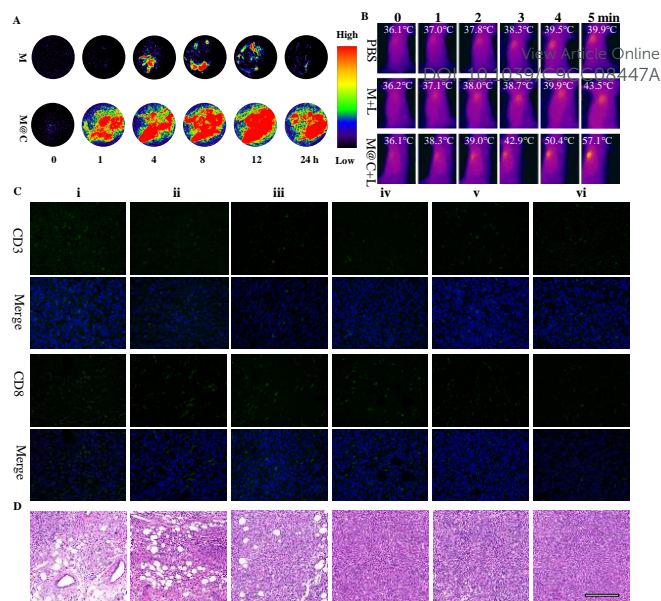


**Figure 3.** In vivo experiments. Photoacoustic images of tumors with M NPs and M@C NPs (A). Photothermal images of mice at 12 h post-injection (B). Immunofluorescent staining images of CD3+ and CD8+ T cells in tumors (C). H&E stained images of tumors, Scale bar = 200  $\mu$ m (D). i-vi represent mice were treated with: (i) M@C+L+IDOi, (ii) M@C+L, (iii) M+L+IDOi, (iv) M@C+IDOi, (v) L, (vi) PBS.

which synergizes immunoblocking inhibitors (IDOi) to provoke a strong and persistent antitumor immune response for enhanced cancer treatment.

M NPs can actively chelate to metal ions with a high loading capacity and stability due to the intrinsic chelating function.<sup>31</sup> M NPs chelated with manganese ions ( $Mn^{2+}$ ) were used to prepare M(Mn)@C NPs. Then 400  $\mu$ g M(Mn)@C NPs were intravenously injected into mice and hearts, livers, spleens, lungs, kidneys and tumors were harvested 12 h later to measure the Mn by ICP-MS. M(Mn)@C NPs distributed in heart, liver, spleen, lung, kidney and tumor were about 0.941, 22.1, 3.35, 4.13, 18.9, 8.00 ID%/g, respectively (Figure S9A). To study the degradation of M@C NPs, feces and urine of mice treated with M(Mn)@C NPs were obtained at different time. As shown in Figure S9B, the materials were gradually flushed out through feces and urine.

The synergetic photothermal-immunological therapeutic effect against breast cancer was assessed in vivo. Details of the therapeutic process were illustrated in Figure 4A. Mice bearing with tumors were treated with (i) M@C+L+IDOi; (ii) M@C+L; (iii) M+L+IDOi; (iv) M@C+IDOi; (v) L; (vi) PBS, respectively. Tumors were exposed to NIR laser of 808 nm (2 W/cm<sup>2</sup>) for 5 min at 12 h post-injection. And IDOi was then injected intraperitoneally at another 12 h post-radiation. Tumors in group (i) grew the slowest, demonstrating an excellent therapeutic effect, while only PTT in group (ii) had moderate therapeutic effect (Figure 4B, C). The corresponding tumor weights were shown in Figure 4D. Body weights (Figure 4E) and H&E stained images of major tissues (Figure S10) indicated the good biocompatibility of all treatments. All results suggest that the photothermal and immunological therapy have the excellent synergy therapeutic effect. Most blood routine indicators in Figure S11 were within normal levels except white blood cells (WBC) in Figure S12. As tumors progress, the inflammation gets worse, which results in

more WBC in the blood (Figure S12). Blood biochemical indexes (ALT, AST, BUN, CRE) after various treatments also showed that all treatments did not damage the liver or kidney (Figure S13).

Tumor metastases are the greatest contributor to patient death, so it is significant to study the therapeutic effect of distance tumors. The design of our animal experiment is shown in Figure S14A. 4T1 cells were inoculated on the left flank of each mouse. Three days later, the second tumor was inoculated on the right flank to mimic the metastatic tumor. Then mice were divided into six groups and treated with: (i) M@C+L+IDOi; (ii) M@C+L; (iii) M+L+IDOi; (iv) M@C+IDOi; (v) L; (vi) PBS, respectively. In groups (i), (ii), (iii) and (v), the light radiation was applied to the left tumors. After 12 h, the IDOi was injected intraperitoneally and tumors were observed every other day. When mice just received PTT, the secondary tumors were delayed to some extent (Figure S14B, C). Moreover, the combination treatment by both M@C+L and IDOi could significantly slow down the growth of secondary tumors, indicating the vital role of combining PTT with immunotherapy. Body weights indicated the good biocompatibility of all treatments in this experiment (Figure S14D). In brief, the M@C NPs with laser in first tumors not only served as photothermal treatment, but also cause the ICD of cancer cells to serve as immunogen. Combining with immunoblocking inhibitors, the strong and persistent antitumor immune response could be retained to inhibit the growth of the secondary tumors.

In summary, we have synthesized the multifunctional materials (M@C NPs) based on natural melanin nanoparticles, which exhibited the superior performance in escape from immune clearance, active tumor-targeting, and PTT-induced ICD. Compared with naked M NPs, M@C NPs converted the M NPs into "smart" agents that were inclined to accumulate in tumors due to the homologous adhesion of cancer cell membrane. Once reached the tumor, M@C NPs acted as the PTT agents for enhanced antitumor immune response by inducing ICD. In combination with immunoblocking inhibitor, M@C NPs showed good therapeutic effect for primary and

abscopal tumors. This strategy can provide guidance for clinical oncology applications. DOI: 10.1039/C9CC08447A

This work was supported by National Natural Science Foundation of China (21535004, 91753111, 21874086, 21390411, 21927811) and the Key Research and Development Program of Shandong Province (2018YFJH0502).

## Conflicts of interest

The authors declare no competing financial interest.

## Notes and references

- J. Couzin-Frankel, *Science*, 2013, **342**, 1432.
- T. N. Schumacher and R. D. Schreiber, *Science*, 2015, **348**, 69.
- P. Sharma, S. Hu-Lieskovan, J. A. Wargo and A. Ribas, *Cell*, 2017, **168**, 707.
- T. F. Gajewski, H. Schreiber and Y. X. Fu, *Nat. Immunol.*, 2013, **14**, 1014.
- A. Ribas and J. D. Wolchok, *Science*, 2018, **359**, 1350.
- P. C. Tumeh, C. L. Harview, J. H. Yearley, I. P. Shintaku, E. J. Taylor, L. Robert and A. N. West, *Nature*, 2014, **515**, 568.
- C. W. Ng, J. Li and K. Pu, *Adv. Funct. Mater.*, 2018, **28**, 1804688.
- K. Kono, K. Mimura and R. Kiessling, *Cell Death & Dis.*, 2013, **4**, e688.
- D. R. Green, T. Ferguson, L. Zitvogel and G. Kroemer, *Nat. Rev. Immunol.*, 2009, **9**, 353.
- G. T. Yu, L. Rao, H. Wu, L. L. Yang, L. L. Bu, W. W. Deng and W. Liu, *Adv. Funct. Mater.*, 2018, **28**, 1801389.
- Z. Zhou, J. Song, L. Nie and X. Chen, *Chem. Soc. Rev.*, 2016, **45**, 6597.
- S. S. Lucky, K. C. Soo and Y. Zhang, *Chem. Rev.*, 2015, **115**, 1990.
- L. Zou, H. Wang, B. He, L. Zeng, T. Tan, H. Cao and Y. Li, *Theranostics*, 2016, **6**, 762.
- Y. Liu, P. Bhattarai, Z. Dai and X. Chen, *Chem. Soc. Rev.*, 2019, **48**, 2053.
- J. Zhang, Y. Guo, F. Ding, G. Pan, X. Zhu and C. Zhang, *Angew. Chem. Int. Ed.*, 2019, DOI: 10.1002/anie.201907380.
- R. M. Slominski, M. A. Zmijewski and A. T. Slominski, *Exp. Dermatol.*, 2015, **24**, 258.
- A. Korner and J. Pawelek, *Science*, 1982, **217**, 1163.
- Y. Liu, K. Ai, J. Liu, M. Deng, Y. He and L. Lu, *Adv. Mater.*, 2013, **25**, 1353.
- Y. Ye, C. Wang, X. Zhang, Q. Hu, Y. Zhang, Q. Liu and G. Dotti, *Sci. Immunol.*, 2017, **2**, eaan5692.
- Z. Yu, P. Zhou, W. Pan, N. Li and B. Tang, *Nat. Commun.*, 2018, **9**, 5044.
- Y. Yang, J. Tang, P. L. Abbaraju, M. Jambhrunkar, H. Song, M. Zhang and C. Yu, *Angew. Chem. Int. Ed.*, 2018, **130**, 11938.
- M. Obeid, A. Tesniere, F. Ghiringhelli, G. M. Fimia, L. Apetoh, J. L. Perfettini and D. Métévier, *Nat. Med.*, 2007, **13**, 54.
- D. V. Krysko, K. S. Ravichandran and P. Vandenabeele, *Nat. Commun.*, 2018, **9**, 4644.
- J. L. Adams, J. Smothers, R. Srinivasan and A. Hoos, *Nat. Rev. Drug Disco.*, 2015, **14**, 603.
- C. Sheridan, *Nat. Biotechnol.*, 2015, **33**, 321.
- E. W. Yue, R. Sparks, P. Polam, D. Modi, B. Douy, B. Wayland and M. Bower, *ACS Med. Chem. Lett.*, 2017, **8**, 486.
- K. Lu, C. He, N. Guo, C. Chan, K. Ni, R. R. Weichselbaum and W. Lin, *J. Am. Chem. Soc.*, 2016, **138**, 12502.
- C. A. Hunter and S. A. Jones, *Nat. Immunol.*, 2015, **16**, 448.
- A. Dittrich, W. Hessenkemper and F. Schaper, *Cytokine & Growth F. R.*, 2015, **26**, 595.
- L. Sun, C. He, L. Nair, J. Yeung and C. E. Egwuagu, *Cytokine*, 2015, **75**, 249.
- Q. Fan, K. Cheng, X. Hu, X. Ma, R. Zhang, M. Yang, X. Lu, L. Xing, W. Huang, S. Gambhir and Cheng, *Z. J. Am. Chem. Soc.*, 2014, **136**, 15185.

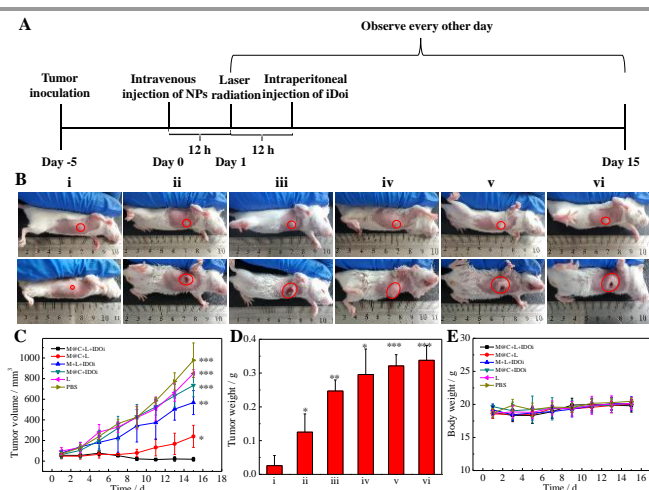


**Figure 4.** Schematic illustration of the in vivo therapeutic process (A). Photographs of the mice before (day 1) and after (day 15) with different treatments: (i) M@C+L+IDOi (ii) M@C+L (iii) M+L+IDOi (iv) M@C+IDOi (v) L (vi) PBS (B). Changes of tumor growth (C) and tumor weights (D), body weights (E) of mice in different groups. P values were calculated using the t-test (\*\*P < 0.01, \*\*\*P < 0.001, \*P < 0.05).